A Signature of Roaming Dynamics in the Thermal Decomposition of Ethyl Nitrite: Chirped-Pulse Rotational Spectroscopy and Kinetic Modeling

Citation: Prozument, Kirill, Yury V. Suleimanov, Beat Buesser, James M. Oldham, William H. Green, Arthur G. Suits, and Robert W. Field. "A Signature of Roaming Dynamics in the Thermal Decomposition of Ethyl Nitrite: Chirped-Pulse Rotational Spectroscopy and Kinetic Modeling." The Journal of Physical Chemistry Letters 5, no. 21 (November 6, 2014): 3641–48.

As Published: http://dx.doi.org/10.1021/jz501758p

Publisher: American Chemical Society (ACS)

Persistent URL: http://hdl.handle.net/1721.1/99150

Version: Author's final manuscript: final author's manuscript post peer review, without publisher's formatting or copy editing

A Signature of Roaming Dynamics in the Thermal Decomposition of Ethyl Nitrite: Chirped-Pulse Rotational Spectroscopy and Kinetic Modeling

Kirill Prozument [1)]*, Yury V. Suleimanov [2)], Beat Buesser [2, 3)], James M. Oldham [4)], William H. Green [2)], Arthur G. Suits [4)], and Robert W. Field [1)]

[1)] Department of Chemistry, Massachusetts Institute of Technology, Cambridge, MA 02139, USA
[2)] Department of Chemical Engineering, Massachusetts Institute of Technology, Cambridge, MA 02139, USA
[3)] IBM Research, Smarter Cities Technology Centre, Dublin 15, Ireland
[4)] Department of Chemistry, Wayne State University, Detroit, MI 48202, USA

September 26, 2014

ABSTRACT

Chirped-pulse (CP) Fourier transform rotational spectroscopy is uniquely suited for near-universal quantitative detection and structural characterization of mixtures that contain multiple molecular and radical species. In this work we employ CP spectroscopy to measure product branching and extract information about the reaction mechanism, guided by kinetic modeling. Pyrolysis of ethyl nitrite, CH_3CH_2ONO, is studied in a Chen type flash pyrolysis reactor at temperatures of 1000–1800 K. The branching between HNO, CH_2O, and CH_3CHO products is measured and compared to the kinetic models generated by the Reaction Mechanism Generator software. We find that roaming $CH_3CH_2ONO \rightarrow CH_3CHO + HNO$ plays an important role in the thermal decomposition of ethyl nitrite, with its rate, at 1000 K, comparable to that of the radical elimination channel $CH_3CH_2ONO \rightarrow CH_3CH_2O + NO$. HNO is a signature of roaming in this system.

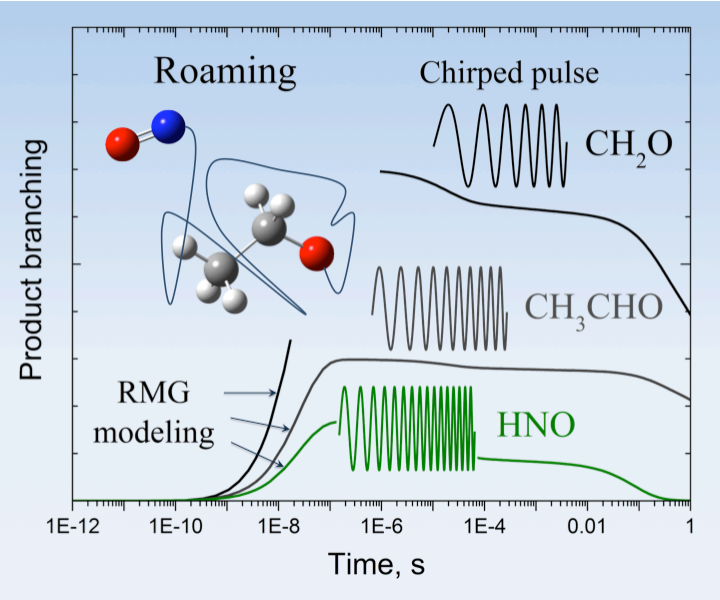

KEYWORDS

Dynamics, kinetics, spectroscopy, roaming, chirped pulse, CPmmW, millimeter wave, microwave, Reaction Mechanism Generator, RMG, Python, RMG-Py, CHEMKIN, unimolecular reaction, transition state theory, branching ratio, reaction yield, molecular beam, pyrolysis, Chen nozzle, combustion, ethyl nitrite, C_2H_5ONO, methyl nitrite, CH_3ONO, nitrosyl hydride, nitroxyl, acetaldehyde, formaldehyde, H_2CO, nitric oxide

Broadband chirped-pulse (CP) Fourier transform rotational spectroscopy, invented by Brooks Pate and coworkers[1-6], has become a standard instrument in molecular spectroscopy laboratories[7-16]. Traditional rotational spectroscopy in the microwave and the millimeter-wave (mm-wave) regions is known for its exceptional resolution, which is ideal for precise determination of molecular structure.[17] A rotational spectrum can also be used to unambiguously identify the species that are produced in a chemical reaction. A principal limitation of the pre-chirped-pulse rotational spectrometer[18-19] for chemical dynamics studies is that it is a narrowband apparatus. A scan over a wide spectral range that includes transitions from more than one species or conformer, may require a prohibitively long time[2] and does not ensure that the line intensities can be meaningfully compared. Broadband chirped-pulse rotational spectroscopy opens new areas of chemical research while retaining the advantages of traditional pure rotational

spectroscopy. Broad spectral regions are covered in a single chirped pulse, with meaningful relative line intensities in the resultant broadband spectra that can be converted to (vibrational state-specific) product branching ratios. CP rotational spectroscopy is a nearly universal (applicable to all polar species) chemical tool that is conformer- and state-specific, quantitative, non-destructive, and suitable for studies of stable and transient species. Pate and coworkers have introduced the CP technique to isomerization dynamics studies by measuring the rate of isomerization between the *syn*- and *anti*- conformations of cyclopropane carboxaldehyderate.[2] CP spectroscopy of nascent photolysis products in multiple vibrational states was demonstrated by Field and coworkers and the approach was proposed for studying transition state(s) properties.[12] Recently, in a series of CP experiments, flash pyrolysis was characterized for rotational and vibrational temperatures of species exiting the reactor and quantitative detection of multiple pyrolysis reaction products was demonstrated.[14]

The roaming mechanism[20-26], is a recently discovered pathway in chemical reactions, which is proving to be a ubiquitous phenomenon observed in unimolecular laser-initiated[20, 27-29] and shock-tube[30-32], and even bimolecular[33] chemistry. In unimolecular decomposition following thermal or laser excitation, the energized precursor molecule (i) may proceed over a barrier, through a conventional tight transition state (TS) on its potential energy surface (PES) to form molecular products: the barriers arise as old chemical bonds are broken and new bonds are formed. Alternatively (ii), a simple bond fission (SBF) reaction may lead to formation of two radicals; since no new bonds are formed, the reaction proceeds without a barrier onto a PES plateau on the product side of the reaction until the radical products are completely separated. Roaming is a third scenario of unimolecular decomposition (iii), in which the system, upon reaching the above-mentioned plateau, reorients and "roams" over the PES while maintaining a few Å separation between the two radical fragments. Eventually, a reactive configuration is found, at which the roaming radicals rearrange into two closed-shell molecular products. The roaming dynamics typically has its threshold in a relatively narrow (~1 kcal/mol) energy window just below the SBF TS, and is associated with a very loose roaming transition state (RTS).

Transition state theory (TST) is commonly used to relate the properties of the TS to reaction rates. There have been proposals[23] to extend TST to include roaming dynamics and several approaches are in development[22-24], but this is a very challenging task. To benchmark these approaches, one needs an experimental method to measure the branching between these three reactive channels, but to-date, even for very small systems, branching measurements between these three reactive pathways has not been achieved. The capability of CP spectroscopy to measure the *branching into multiple products*, and, through that, the related reaction rates, may prove to be a decisive technique for revealing roaming reaction mechanisms. The vibrational population distribution of photolysis[12] products is also measurable in a CP experiment, and encodes the properties of a TS. However, when studying complex chemistry involving secondary and higher order reactions that follow the initial unimolecular decomposition event, kinetic modeling will also be essential to extract the reaction rates from the measured product concentrations.

In this Letter we use CP spectroscopy to detect and quantify three reaction products and, by means of kinetic simulation, show that the observed yield of nitrosyl hydride (HNO) relative to other products in the pyrolysis of ethyl nitrite (CH_3CH_2ONO) is evidence for roaming dynamics. The other two products that we measure are formaldehyde (CH_2O) and acetaldehyde (CH_3CHO). A similar system, methyl nitrite (CH_3ONO) was studied in a recent theoretical work and a roaming mechanism for $CH_3ONO \rightarrow CH_2O + HNO$ molecular elimination was suggested.[34] We employ the Reaction Mechanism Generator (RMG) software that has been demonstrated to be a reliable tool for modeling complex chemical reactions.[35] Introducing the roaming mechanisms into the model can affect, in a major way, the predicted rates of some reactions and thus the concentrations of products predicted by the model. We find a unique set of reaction rates that reproduces the measured branching between the HNO, CH_2O, and CH_3CHO products of CH_3CH_2ONO pyrolysis, and through that learn about the underlying dynamics and estimate the contributions of various mechanisms in the thermal decomposition of ethyl nitrite.

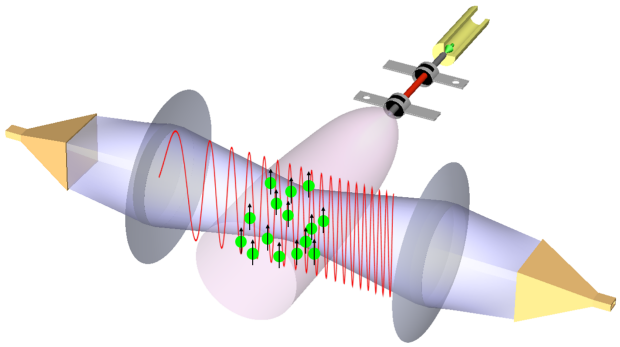

Figure 1. Experimental setup schematic. The molecules exiting the heated tubular reactor expand supersonically into vacuum and are probed by the mm-wave beam of the CPmmW spectrometer. The interaction region is situated in the collision-free zone of the expansion and is represented as a cloud of polarized molecules. The mm-wave beam is broadcast by a horn antenna and is focused into the interaction region by a Teflon lens. The frequency of the mm-wave beam is swept linearly in time (chirped) as illustrated schematically by the wave in the figure. The other lens and the horn collect the free induction decay (FID) emitted by the polarized molecular rotational transitions. The FID is digitized by the CPmmW spectrometer and Fourier-transformed to a frequency domain rotational spectrum that contains the transitions, including their relative intensities, of all species covered by the chirp.[8, 14] Reproduced from Ref. [14] by permission of the PCCP Owner Societies.

The experimental setup (Fig. 1), consisting of the Chirped-Pulse millimeter-Wave (CPmmW) spectrometer[8] coupled to a Chen type nozzle[36-39], was discussed in detail in a recent publication[14] and some relevant aspects are reviewed in the Experimental Methods section. The precursor ethyl nitrite molecules, entrained in argon gas at 0.1% by mole, are introduced into the

reactor by a pulsed valve that operates at the stagnation pressure p_0 = 3 bar. After passing through the heated SiC tube, in which the pyrolysis reactions take place, the products and remaining precursor molecules expand supersonically into the vacuum chamber and can be measured by the CPmmW spectrometer. The CPmmW spectra of the CH_2O, CH_3CHO, and HNO products of ethyl nitrite pyrolysis and the corresponding branching ratio were previously observed at the reactor wall temperature T_{wall} = 1500 K.[14]

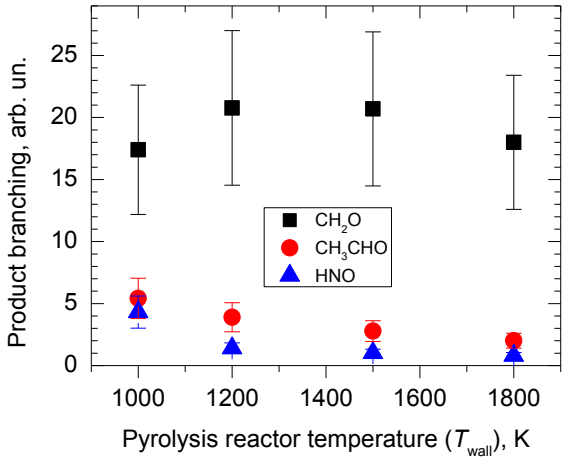

Figure 2. Branching of the ethyl nitrite pyrolysis products determined in the CPmmW experiment. The relative concentrations of CH_2O (black squares), CH_3CHO (red circles), and HNO (blue triangles), measured at the reactor temperature T_{wall} of 1000, 1200, 1500, and 1800 K are displayed with the experimental uncertainties.

In order to investigate the chemistry inside the reactor, we measured the branching ratios of the three products of CH_3CH_2ONO pyrolysis at various reactor temperatures. In Fig. 2 the relative concentrations of the three products, HNO, CH_2O, and CH_3CHO are shown at T_{wall} = 1000, 1200, 1500, and 1800 K. In the present work we are only concerned with relative concentrations of products or branching ratios and leave analysis of the absolute concentrations for future studies.

The residence time of the molecules inside the reactor is estimated[39] to be ~100 μs, which, as discussed below and in the Supporting Information (SI) section, is sufficient, at elevated temperatures, for both the initial unimolecular decomposition of ethyl nitrite and the subsequent chemistry to take place. It was proposed in the earlier ethyl nitrite pyrolysis studies[37, 40-42] that formaldehyde and acetaldehyde products can result from a SBF radical elimination reaction

$$CH_3CH_2ONO \xrightarrow{SBF} CH_3CH_2O + NO, \qquad \text{(Rxn 1)}$$

followed by fast dissociation of the ethoxy radical (CH_3CH_2O) via either of two channels:

$$CH_3CH_2O \rightarrow CH_2O + CH_3 \quad \text{(Rxn 2)}$$

or

$$CH_3CH_2O \rightarrow CH_3CHO + H. \quad \text{(Rxn 3)}$$

The mechanism leading to the formation of HNO is less certain. It may involve abstraction of H-atoms by free NO radicals

$$CH_3CH_2O + NO \rightarrow CH_3CHO + HNO, \quad \text{(Rxn 4)}$$

$$RH + NO \rightarrow R + HNO, \quad \text{(Rxn 5)}$$

conventional unimolecular decomposition via a tight TS

$$CH_3CH_2ONO \xrightarrow{\text{tight TS}} CH_3CHO + HNO, \quad \text{(Rxn 6)}$$

or the NO radical roaming pathway

$$CH_3CH_2ONO \xrightarrow{\text{RTS}} CH_3CHO + HNO. \quad \text{(Rxn 7)}$$

While reactions 1–6 are commonly accepted, additional, unknown reaction pathways may be responsible for the observed product yields. In order to correctly describe the kinetics in the flash pyrolysis reactor, the Python version of the Reaction Mechanism Generator (RMG-Py) software[35] has been used to explore the complete reaction network. The automated procedure implemented in RMG-Py for kinetic model generation is designed to avoid the process of constructing kinetic models manually, which can be error-prone and can often lead to wrong conclusions. The principles of RMG-Py modeling and the details of the present simulation are described in the Computational Methods section.

As output, RMG-Py automatically generates all possible reaction pathways and constructs a comprehensive (CHEMKIN[43]-format) list of relevant elementary reaction steps, including values of reaction rate constants and thermochemical properties. CHEMKIN simulations were performed in an isobaric homogeneous batch reactor model. We appreciate that such a model is an oversimplification of the real reactor used in the present experiment. The sufficiency of this model to the goal of understanding the role of roaming dynamics in the present system is discussed below. Computational fluid dynamics (CFD) simulations of continuous flow through a similar SiC tubular reactor,[39] and measurements in a different type of pyrolysis reactor,[44] show a pressure drop toward the end of the tube, and temperature variations. We found that, at lower temperatures, the product distribution profiles do not change within the selected pressure region and use the values of the average pressure, p = 0.5 bar, and the temperature, $T = T_{wall}$, inside the reactor.

The list of the key chemical reactions that generate and consume the three observed products, CH_2O, CH_3CHO, and HNO are summarized in Part 1 of the SI and the CHEMKIN file

containing all the reactions considered in the model generated by RMG-Py is supplied in the SI. RMG-Py confirms the key role of all Rxns 1–6 indicated above. However, the roaming unimolecular dissociation (Rxn 7) requires special treatment. Roaming paths have not been a part of the RMG-Py reaction family set and the rate of Rxn 7 is not well-known. The nature of this reaction, as discussed above, is intimately related to the radical elimination channel (Rxn 1). Therefore, in order to introduce the roaming mechanism to the kinetic simulation, we adopt the following simple model of proportionality between the rates of Rxn 1 (radical dissociation channel) and Rxn 7 (roaming channel)

$$\alpha(T) = \frac{k(\mathrm{CH_3CH_2ONO} \xrightarrow{\mathrm{RTS}} \mathrm{CH_3CHO + HNO})}{k(\mathrm{CH_3CH_2ONO} \xrightarrow{\mathrm{SBF}} \mathrm{CH_3CH_2O + NO})} \quad , \qquad \text{(Eq 1)}$$

with $\alpha(T)$ as the proportionality coefficient, which is, in general, a function of temperature. All RMG-Py calculations were repeated for different values of α and the results at T = 1000 and 1500 K are displayed in Fig. 3 (the simulation results at other temperatures and pressures are available in the SI). Each panel shows the time evolution of the concentrations of CH_2O, CH_3CHO, and HNO at a certain temperature, T. The $t = 10^{-4}$ s time point corresponds to the residence time in the reactor and thus the product branching at $t = 10^{-4}$ s can be compared to the experimentally measured branching in Fig. 2.

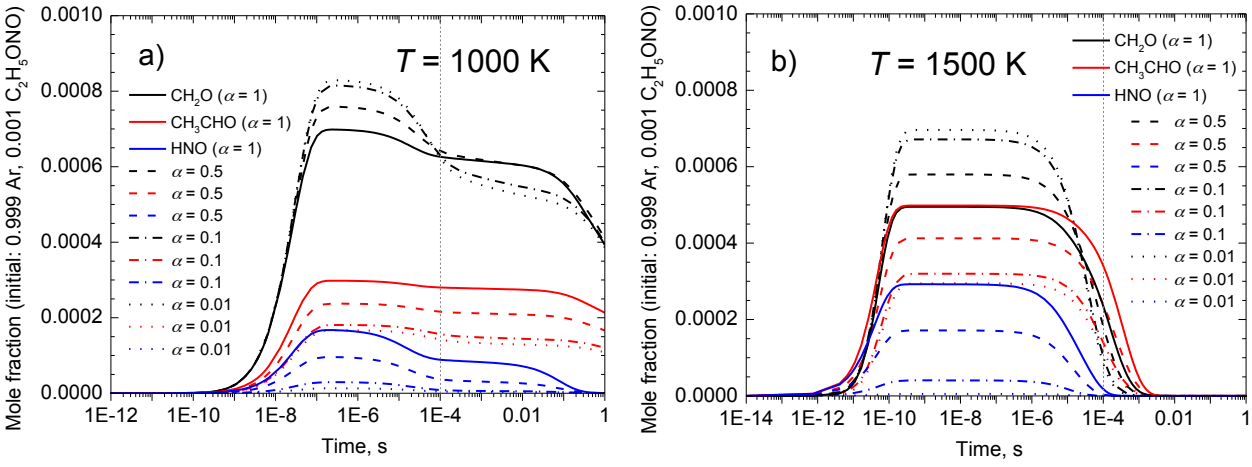

Figure 3. RMG-Py simulations at temperatures a) T = 1000 K and b) 1500 K and p = 0.5 bar: CH_2O, CH_3CHO, and HNO mole fraction (product concentration) distribution as a function of time for different values of α and reactor temperatures. Plateau regions of the mole fraction profiles do not change qualitatively at other pressures in the 0.1–3 bar range (see SI, Part 3). The dotted vertical lines in each panel indicate the 100 μs time point at which the molecules exit the reactor in our experiment. The intersections of the CH_2O, CH_3CHO, and HNO traces with the 100

μs line indicate the mole fractions relevant to this experiment and can be compared with the measured branching in Fig. 2.

The best agreement between the experiment and the model is achieved at lower reactor temperatures. For example, at T = 1000 K and α = 1, (Fig. 3a) the branching ratio CH_2O : CH_3CHO : HNO = 17.5 : 5.5 : 4.5 is close to that of Fig. 2 at T_{wall} = 1000 K. Decomposition of ethyl nitrite starts at $t = 10^{-9}$ s and by the $t = 10^{-7}$ s time point, formation of CH_2O, CH_3CHO, and HNO, and decomposition of CH_3CH_2ONO are complete. An important observation is that, according to our kinetic model, *bimolecular chemistry* that sets in at about $t = 10^{-5}$ s consumes the three products and *does not produce* HNO. Therefore the observed HNO product is formed in a fast unimolecular decomposition reaction via a roaming path (Rxn 7), or through a tight TS[45] (Rxn 6). Roaming is expected to have a much larger reaction rate because of both the entropic[46-47] and energetic[25, 34] factors: proceeding via a loose RTS, a system samples a much greater configuration space than when dissociating through a conventional tight TS; in addition, the latest calculations[34] of the CH_3NO_2/CH_3ONO system place the RTS in the $CH_3ONO \rightarrow CH_2O$ + HNO reaction 6.8 kcal/mol lower in energy than the corresponding tight TS. Indeed, in Fig. 3a, when the parameter α is set to smaller values, effectively "switching off" the roaming mechanism, the predicted concentration of HNO at $t = 10^{-4}$ s decreases to a level far below what is observed experimentally. The *roaming mechanism* (Rxn 7) that is introduced into the kinetic model via Eq. 1 *is required*, with $\alpha \sim 1$, for agreement between theory and experiment. Lin and coworkers, in their recent calculations of thermal decomposition of methyl nitrite[34], come to a similar conclusion: the SBF and the roaming channels are of equal importance for HNO formation (see Fig. 7 in their work).

The temperature distribution inside the reactor is likely to be non-uniform with the regions adjacent to the reactor wall heated up to T_{wall} and with colder core flow at $T < T_{wall}$.[14, 48] In order to account for possible contributions of colder layers, the T = 600 and 800 K simulations are provided in the SI. Whereas no chemistry takes place before $t \sim 1000$ μs at T = 600 K, roaming with $\alpha > 1$ is required for modeling the T = 800 K flow layer inside the tube heated to T_{wall} = 1000 K. Therefore, even (and especially) if HNO is formed in the colder regions of the reactor at $T < T_{wall}$, it signifies the roaming mechanism. Variation of the pressure within the $0.1 \leq p \leq 3$ bar range has only a minor effect on the results of the simulation at T = 1000 K (see Figs. S2 and S3 in the SI). Even at the highest possible pressure in the SiC tube of $p = p_0 = 3$ bar, bimolecular chemistry does not produce a significant amount of HNO, CH_2O or CH_3CHO.

The RMG model leads to an important understanding of the kinetics at hand: the CH_2O : CH_3CHO : HNO *branching ratio* is defined during the initial exponentially fast formation of products ($10^{-8} \leq t \leq 10^{-7}$ s in Fig. 3a) by a set of unimolecular decompositions (Rxns. 1, 2, 3, 7) and remains steady during the subsequent plateaus of concentration ($10^{-7} \leq t \leq 10^{-2}$ s in Fig. 3a), with some perturbation due to product consumption. Because the branching ratios are formed

very quickly and remain constant for extended periods of time, the current model is applicable even if the effective residency time t_{rxn} during which the reactions occur is different from 100 μs. Since similar branching ratios are observed for all reactor pressures considered, this suggests the results of the current model, which assumes a constant pressure throughout the reactor, would be immune to the effects of pressure dropping along the reactor axis that are predicted[48] by the CFD calculations. We estimate that as long as the effective conditions in the reactor when T_{wall} = 1000 K are within the $800 \leq T \leq 1000$ K, $0.1 \leq p \leq 3$ bar, $1 \leq t_{rxn} \leq 1000$ μs volume of the (T, p, t_{rxn}) parameter space, the measured CH_2O : CH_3CHO : HNO branching ratio is described by the kinetic model in which most of the HNO product is formed by NO radical roaming in the thermal decomposition of CH_3CH_2ONO. Once the conditions in the reactor can be controlled with more certainty, it would be interesting to experimentally investigate the subtle question[34] of how the *unimolecular* roaming pathway depends on pressure. Collisions with argon atoms may quench the roaming NO radical and shift the product branching from Rxn 7 to Rxn 1. In the present study this effect is implicitly included in the $\alpha(T)$ parameter.

At higher temperatures (T = 1500 K in Fig. 3b, and T = 1200–1800 K in the SI, Parts 2 and 3) inside the reactor, we obtain poorer agreement of the predicted CH_2O and CH_3CHO concentrations with experiment. Likely contributors to this discrepancy are the rate constants for the ethoxy decomposition used in the present model, specifically those for the branching between Rxns 2 and 3. Although the rates from Batt[49-50] measured at 393 – 433 K give more satisfactory agreement with our experiment, we use the data from the compilation of Curran[50-51] for consistency with the other reaction rates that are taken from Ref.[50-51]. At elevated temperatures it is also the case that smaller α, within the $0.1 < \alpha < 1$ range, are required to explain the measured HNO branching ratio. This is in accordance with the calculated increase of roaming branching at lower, near-threshold energies in a microcanonical ensemble[21-23, 25], and the observed temperature behavior of roaming in shock-tube experiments[31-32].

An important consideration in these experiments is the poorly-understood role of wall reactions in the SiC tube that are capable of skewing the product distribution. The possibility of wall reactions was considered in a previous investigation[52] by isotope scrambling experiments, leading to the conclusion that wall reactions were not an important factor in that study. A new CFD investigation[48] calculates the characteristic time of diffusion of acetaldehyde molecules to the wall of the reactor and concludes that it is less, but comparable to the residence time. In principle, there is a possibility for NO radicals that are formed in Rxn 1 to abstract an H-atom that may reside on the wall and form the HNO product.

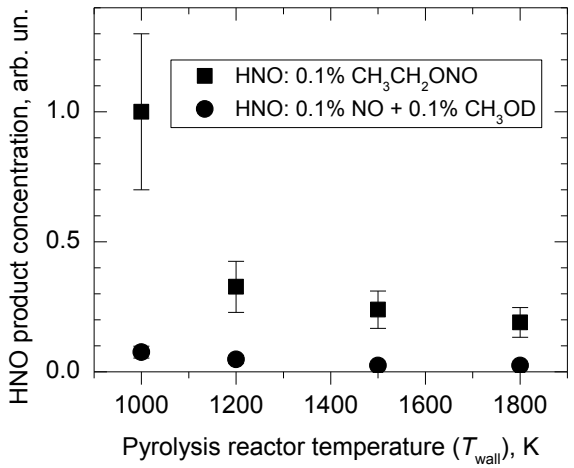

Figure 4. The yield of HNO in the pyrolysis of 0.1% CH_3CH_2ONO + 99.9% argon (squares), and in the pyrolysis of 0.1% NO + 0.1% CH_3OD + 99.8% argon (circles) measured at the reactor temperature T_{wall} of 1000, 1200, 1500, and 1800 K. Displayed with the experimental uncertainties.

To elucidate the possible contributions of non-unimolecular mechanisms of HNO formation we conducted a set of additional measurements. NO gas was pre-mixed with CH_3OD in argon with mole fractions 0.1% NO + 0.1% CH_3OD + 99.8% Ar, and expanded through the reactor at various temperatures. The observed yield of HNO is plotted in Fig. 4 and compared to the results of ethyl nitrite pyrolysis. A DNO signal was not observed. Direct H-atom abstraction $CH_3OD + NO \rightarrow CH_2OD + HNO$ is expected to be slow and the observed HNO is likely to be associated with the wall reactions. Thus the NO and CH_3OD mixture measurements suggest that wall reactions can be responsible for $\lesssim$10% of HNO formed in the ethyl nitrite pyrolysis experiments described in this work. Although the wall-mediated reactions are likely to be present, they are expected to make only a minor contribution that is on a par with other uncertainties in the present study.

In summary, we suggest that the roaming mechanism plays an important role in the thermal decomposition of ethyl nitrite. The $CH_3CH_2ONO \xrightarrow{RTS} CH_3CHO + HNO$ reaction, proceeding via NO radical roaming, is found to be responsible for the appearance of most of the HNO product. We estimate that at the reactor temperature of T_{wall} = 1000 K the rate of decomposition by roaming, $CH_3CH_2ONO \xrightarrow{RTS} CH_3CHO + HNO$, is of the same order of magnitude as the rate of simple bond fission reaction $CH_3CH_2ONO \xrightarrow{SBF} CH_3CH_2O + NO$. Other reactions (unimolecular or bimolecular) are found not to make a significant contribution to the thermal decomposition of ethyl nitrite. Quantitative and nearly universal detection of multiple reaction products by chirped-pulse Fourier transform rotational spectroscopy in combination with accurate kinetic modeling has shown to be a fruitful approach to studying molecular dynamics and kinetics of complex systems.

The development of the CP method to the study of pyrolysis reactions in a Chen type nozzle will benefit from several improvements. The significance, and mechanisms, of wall reactions need to be clarified in more detail. Applying calculated[48] or measured temperature and pressure fields in RMG-Py and CHEMKIN simulations will be a further major improvement in the accuracy of the modeling part of the present type of experiments. Establishing more subtle properties of roaming dynamics through the exact value of the α parameter and its temperature and pressure dependencies would then be within reach. The rates of the crucial reactions, such as Rxns 2 and 3 in the present work, can be measured or calculated *ab initio* to improve the agreement between the measured and predicted CH_2O : CH_3CHO branching ratios.

Understanding the role of roaming in thermally induced reactions is important for combustion and biomass pyrolysis research and applications. Roaming is now known to be a ubiquitous phenomenon with sizable branching that needs to be considered in accurate kinetic modeling along with the conventional molecular and radical elimination mechanisms. A further investigation of roaming dynamics in the pyrolysis of ethyl nitrite, as well as methyl nitrite and nitromethane would be possible and desirable. Detecting and quantifying additional pyrolysis products such as CO and NO would further facilitate gauging kinetic models against the CP measurements. Other chemical systems that may be studied using the combination of CP spectroscopy and kinetic modeling are pyrolysis of esters and carboxylic acids that are of importance for combustion research. Investigations of roaming in acetaldehyde, propanal and acetone are also within reach.

EXPERIMENTAL METHODS

The Chen type flash pyrolysis reactor[36] used in the present work, similar to the reactor used in the Ellison research group[37-39]. The reactor is a 5.7 cm long 1 mm i.d. SiC tube mounted inside the vacuum chamber that operates at 2.5×10^{-5} mbar pressure. The 3.2 cm long section of the tube can be resistively heated to wall temperatures of T_{wall} = 1000–1800 K that is measured by an optical pyrometer with the experimental uncertainty of ± 100 K.

Despite the high temperature of the SiC reactor, the molecules are efficiently cooled in the expansion to rotational temperatures of T_{rot} = 4 ± 1 K[14] and can be studied by rotational spectroscopy. While rotational relaxation is considered to be fast for most species, vibrational relaxation is highly dependent on the molecule's vibrational energy level separations, symmetry and couplings.[14] Unlike in the slit jet experiments[12] where nascent vibrational population distributions are available for investigation, heavy rotation-vibration cooling in the expansion from the flash pyrolysis reactor imprints on the vibrational level population. Scrambling of the nascent vibrational population information is compensated by the efficient rotational cooling in the present flash pyrolysis experiments, which facilitates rotational thermalization of reaction products and allows for product branching to be quantified.

To maximize the overlap between the mm-wave beam and the molecular sample in the collision-free zone of the expansion (Fig. 1), where the molecules reach their terminal rotational temperature T_{rot}, no skimmer is used in this experiment. A CPmmW spectrometer[8, 14] that operates in the 63–102 GHz spectral region is utilized in this work in the multi-chirp[14] mode of operation. Preference is given to the mm-wave spectral region[4, 6, 8] over the more commonly used microwave region (2–50 GHz) in order to observe the more intense, at $T_{rot} = 4 \pm 1$ K, $J_{KaKc} = 1_{01}–0_{00}$ rotational transitions[53-54] of small (2 heavy atoms) molecules, such as CH_2O and HNO, and also higher-J transitions of larger molecules.

Conversion of the experimentally observed rotational line intensities to product concentrations is performed[14] using the PGOPHER[54] software, which is set to include the rotational levels' population differences in the intensity calculations. A rotational temperature of $T_{rot} = 4 \pm 1$ K measured for the acetaldehyde product molecules is assumed to be common to all species in the interaction region.[14] The other required parameters are permanent electric dipole moments[53] that are converted to transition electric dipole moments[17], and the chirp bandwidths and their duration.

COMPUTATIONAL METHODS

RMG-Py is a rate-rule-based reaction network generator that constructs reaction networks at given conditions (temperature, pressure, initial concentration) and user-defined tolerances for accuracy. RMG-Py estimates the high pressure kinetics using over 40 reaction family templates filled with representative kinetics (e.g. H-abstraction, radical recombination, β-scission) including recently added nitrogen chemistry. This is supported by vast libraries of measured and calculated rates. RMG-Py constructs reaction mechanisms in a hierarchical manner. Starting from a seed mechanism, it continues extending the mechanism by searching for new reactions until all newly found reactions are slower than a predefined fraction of the characteristic rate constant of the overall mechanism. A seed mechanism is defined as a list of species, reactions, and rate coefficients that will remain part of the reaction mechanism and contains mostly small molecule reactions that are not well captured by characteristic rates defined in reaction families, which apply better for larger molecules, but that are essential for phenomena like ignition. The RMG-Py software then proposes new reactions, using the list of species supplied in the seed mechanism and the new larger molecules of interest, by comparing each combinatorial possibility against the reaction family templates in the RMG-Py database. A complete and continuously expanding list of reaction family templates can be found online.[35] Any reactions composed exclusively of those species in the seed mechanism are added to the core of the reaction mechanism (the "cross-reactions"); all others are added to the edge of the reaction mechanism. Application of the rate-based algorithm[55] for the temperature, pressure, and species' concentrations of interest, until the user-specified tolerance is satisfied, results in the final chemical kinetic model.

In the present case, the seed mechanism consists of small-molecule chemistry that originates from the EFRC Foundation Fuel Mechanism v.0.9[56] and several nitrogen chemistry mechanisms.[50, 57-60] The simulation was run at pressures of 0.1, 0.5, and 3 bar and temperatures T = 600, 800, 1000, 1200, 1500, and 1800 K to include low and high temperature chemistry in the model and for initial mole fractions of 0.001 for ethyl nitrite and 0.999 for Ar to mimic the conditions of the experiment. Pressure dependent kinetics has been estimated by the Modified Strong Collision approach,[61] using estimates of $\rho(E)$ described by Allen *et al* [62]. The thermochemistry of all species is either supplied by thermochemical libraries or estimated using Benson's group additivity scheme.[63] Transport properties, such as Lennard-Jones parameters, are estimated using an empirical relationship that depends on a species' critical temperature and pressure.[64] The termination criterion was 0.99% conversion of the initial reactants in all cases.

AUTHOR INFORMATION

Corresponding Author

*E-mail: prozument@mit.edu

Notes

The authors declare no competing financial interest.

ACKNOWLEDGMENTS

We thank Prof. Barney Ellison for his assistance in development of the MIT pyrolysis experiment. KP acknowledges the Donors of the American Chemical Society Petroleum Research Fund for support under the grant number 50650-ND6. RWF and KP acknowledge the personnel and equipment support by the U.S. Department of Energy, Office of Basic Energy Sciences under Award Number DEFG0287ER13671. Y.V.S. and W.H.G. acknowledge the support of the Combustion Energy Frontier Research Center, an Energy Frontier Research Center funded by the U.S. Department of Energy, Office of Basic Energy Sciences under Award Number DE-SC0001198. AGS acknowledges the Army Research Office award number 58245-CH-11 for financial support. B.B. acknowledges gratefully the financial support from the Swiss National Science Foundation (SNF) Postdoctoral Research Grant PBEZB2-140081.

SUPPORTING INFORMATION AVAILABLE

The rates of some reactions that are used in the present RMG-Py model are given in Part 1 of the Supporting Information. The results of the RMG-Py simulation at temperatures T = 600, 800,

1000, 1200, 1500, 1800 K and α = 0.01. 0.1, 0.5, 1 and the pressure p = 0.5 bar are shown in Part 2. The RMG-Py modeling results at p = 0.1, 0.5, 3 bar, T = 1000, 1200, 1500, 1800 K, and α = 0.01, 1 are shown in Part 3. The CHEMKIN file is supplied. This material is available free of charge via the Internet http://pubs.acs.org.

REFERENCES

(1) Brown, G. G.; Dian, B. C.; Douglass, K. O.; Geyer, S. M.; Shipman, S. T.; Pate, B. H. A Broadband Fourier Transform Microwave Spectrometer Based on Chirped Pulse Excitation. *Rev. Sci. Instrum.* **2008**, *79*, 053103.

(2) Dian, B. C.; Brown, G. G.; Douglass, K. O.; Pate, B. H. Measuring Picosecond Isomerization Kinetics via Broadband Microwave Spectroscopy. *Science* **2008**, *320*, 924-928.

(3) Neill, J. L.; Douglass, K. O.; Pate, B. H.; Pratt, D. W. Next Generation Techniques in the High Resolution Spectroscopy of Biologically Relevant Molecules. *Phys. Chem. Chem. Phys.* **2011**, *13*, 7253-7262.

(4) Steber, A. L.; Harris, B. J.; Neill, J. L.; Pate, B. H. An Arbitrary Waveform Generator Based Chirped Pulse Fourier Transform Spectrometer Operating from 260 to 295 GHz. *J. Mol. Spectrosc.* **2012**, *280*, 3-10.

(5) Zaleski, D. P.; Neill, J. L.; Muckle, M. T.; Seifert, N. A.; Carroll, P. B.; Weaver, S. L. W.; Pate, B. H. A K-a-Band Chirped-Pulse Fourier Transform Microwave Spectrometer. *J. Mol. Spectrosc.* **2012**, *280*, 68-76.

(6) Neill, J. L.; Harris, B. J.; Steber, A. L.; Douglass, K. O.; Plusquellic, D. F.; Pate, B. H. Segmented Chirped-Pulse Fourier Transform Submillimeter Spectroscopy for Broadband Gas Analysis. *Opt. Express* **2013**, *21*, 19743-19749.

(7) Karunatilaka, C.; Shirar, A. J.; Storck, G. L.; Hotopp, K. M.; Biddle, E. B.; Crawley, R.; Dian, B. C. Dissociation Pathways of 2,3-Dihydrofuran Measured by Chirped-Pulse Fourier Transform Microwave Spectroscopy. *J. Phys. Chem. Lett.* **2010**, *1*, 1547-1551.

(8) Park, G. B.; Steeves, A. H.; Kuyanov-Prozument, K.; Neill, J. L.; Field, R. W. Design and Evaluation of a Pulsed-Jet Chirped-Pulse millimeter-Wave Spectrometer for the 70-102 GHz Region. *J. Chem. Phys.* **2011**, *135*, 024202.

(9) Pate, B. H.; De Lucia, F. C. Broadband Molecular Rotational Spectroscopy Special Issue Introduction. *J. Mol. Spectrosc.* **2012**, *280*, 1-2.

(10) Schnell, M. Broadband Rotational Spectroscopy for Molecular Structure and Dynamics Studies. *Z. Phys. Chem.* **2013**, *227*, 1-21.

(11) Perez, C.; Lobsiger, S.; Seifert, N. A.; Zaleski, D. P.; Temelso, B.; Shields, G. C.; Kisiel, Z.; Pate, B. H. Broadband Fourier Transform Rotational Spectroscopy for Structure Determination: The Water Heptamer. *Chem. Phys. Lett.* **2013**, *571*, 1-15.

(12) Prozument, K.; Shaver, R. G.; Ciuba, M. A.; Muenter, J. S.; Park, G. B.; Stanton, J. F.; Guo, H.; Wong, B. M.; Perry, D. S.; Field, R. W. A New Approach toward Transition State Spectroscopy. *Faraday Discuss.* **2013**, *163*, 33-57.

(13) Seifert, N. A.; Zaleski, D. P.; Perez, C.; Neill, J. L.; Pate, B. H.; Vallejo-Lopez, M.; Lesarri, A.; Cocinero, E. J.; Castano, F.; Kleiner, I. Probing the C-H Weak Hydrogen Bond in Anesthetic Binding: The Sevoflurane-Benzene Cluster. *Angew. Chem. Int. Edit.* **2014**, *53*, 3210-3213.

(14) Prozument, K.; Park, G. B.; Shaver, G. R.; Vasiliou, A. K.; Oldham, J. M.; David, D. E.; Muenter, J. S.; Stanton, J. F.; Suits, A. G.; Ellison, G. B.; Field, R. W. Chirped-Pulse millimeter-Wave Spectroscopy for Dynamics and Kinetics Studies of Pyrolysis Reactions. *Phys. Chem. Chem. Phys.* **2014**, *16*, 15739-15751.

(15) Patterson, D.; Schnell, M. New Studies on Molecular Chirality in the Gas Phase: Enantiomer Differentiation and Determination of Enantiomeric Excess. *Phys. Chem. Chem. Phys.* **2014**, *16*, 11114-11123.

(16) Kidwell, N. M.; Vaquero-Vara, V.; Ormond, T. K.; Buckingham, G. T.; Zhang, D.; Mehta-Hurt, D. N.; McCaslin, L.; Nimlos, M. R.; Daily, J. W.; Dian, B. C.; Stanton, J. F.; Ellison, G. B.; Zwier, T. S. Chirped-Pulse Fourier Transform Microwave Spectroscopy Coupled with a Flash Pyrolysis Microreactor: Structural Determination of the Reactive Intermediate Cyclopentadienone. *J. Phys. Chem. Lett.* **2014**, *5*, 2201-2207.

(17) Townes, C. H.; Schawlow, A. L. *Microwave Spectroscopy*. McGraw Hill Book Company: New York, **1955**.

(18) Balle, T. J.; Flygare, W. H. Fabry-Perot Cavity Pulsed Fourier-Transform Microwave Spectrometer with a Pulsed Nozzle Particle Source. *Rev. Sci. Instrum.* **1981**, *52*, 33-45.

(19) Suenram, R. D.; Grabow, J. U.; Zuban, A.; Leonov, I. A Portable, Pulsed-Molecular-Beam, Fourier-Transform Microwave Spectrometer Designed for Chemical Analysis. *Rev. Sci. Instrum.* **1999**, *70*, 2127-2135.

(20) Townsend, D.; Lahankar, S. A.; Lee, S. K.; Chambreau, S. D.; Suits, A. G.; Zhang, X.; Rheinecker, J.; Harding, L. B.; Bowman, J. M. The Roaming Atom: Straying from the Reaction Path in Formaldehyde Decomposition. *Science* **2004**, *306*, 1158-1161.

(21) Zhang, X. B.; Rheinecker, J. L.; Bowman, J. M. Quasiclassical Trajectory Study of Formaldehyde Unimolecular Dissociation: $H_2CO \rightarrow H_2 + CO$, $H + HCO$. *J. Chem. Phys.* **2005**, *122*, 114313.

(22) Suits, A. G. Roaming Atoms and Radicals: A New Mechanism in Molecular Dissociation. *Acc. Chem. Res.* **2008**, *41*, 873-881.

(23) Klippenstein, S. J.; Georgievskii, Y.; Harding, L. B. Statistical Theory for the Kinetics and Dynamics of Roaming Reactions. *J. Phys. Chem. A* **2011**, *115*, 14370-14381.

(24) Bowman, J. M.; Shepler, B. C. Roaming Radicals. *Annu. Rev. Phys. Chem.* **2011**, *62*, 531-553.

(25) Homayoon, Z.; Bowman, J. M. Quasiclassical Trajectory Study of CH_3NO_2 Decomposition via Roaming Mediated lsomerization Using a Global Potential Energy Surface. *J. Phys. Chem. A* **2013**, *117*, 11665-11672.

(26) Bowman, J. M. Roaming. *Mol. Phys.* **2014**, (DOI:10.1080/00268976.2014.897395).

(27) Houston, P. L.; Kable, S. H. Photodissociation of Acetaldehyde as a Second Example of the Roaming Mechanism. *Proc. Natl. Acad. U. S. A.* **2006**, *103*, 16079-16082.

(28) Grubb, M. P.; Warter, M. L.; Xiao, H. Y.; Maeda, S.; Morokuma, K.; North, S. W. No Straight Path: Roaming in Both Ground- and Excited-State Photolytic Channels of $NO_3 \rightarrow NO + O_2$. *Science* **2012**, *335*, 1075-1078.

(29) Dey, A.; Fernando, R.; Abeysekera, C.; Homayoon, Z.; Bowman, J. M.; Suits, A. G. Photodissociation Dynamics of Nitromethane and Methyl Nitrite by Infrared Multiphoton Dissociation Imaging with Quasiclassical Trajectory Calculations: Signatures of the Roaming Pathway. *J. Chem. Phys.* **2014**, *140*, 054305.

(30) Sivaramakrishnan, R.; Michael, J. V.; Klippenstein, S. J. Direct Observation of Roaming Radicals in the Thermal Decomposition of Acetaldehyde. *J. Phys. Chem. A* **2010**, *114*, 755-764.

(31) Sivaramakrishnan, R.; Michael, J. V.; Wagner, A. F.; Dawes, R.; Jasper, A. W.; Harding, L. B.; Georgievskii, Y.; Klippenstein, S. J. Roaming Radicals in the Thermal Decomposition of Dimethyl Ether: Experiment and Theory. *Combust. Flame* **2011**, *158*, 618-632.

(32) Sivaramakrishnan, R.; Michael, J. V.; Harding, L. B.; Klippenstein, S. J. Shock Tube Explorations of Roaming Radical Mechanisms: The Decompositions of Isobutane and Neopentane. *J. Phys. Chem. A* **2012**, *116*, 5981-5989.

(33) Joalland, B.; Shi, Y.; Kamasah, A.; Suits, A. G.; Mebel, A. M. Roaming Dynamics in Radical Addition–Elimination Reactions. *Nat. Commun.* **2014**, *5*, 4064.

(34) Zhu, R. S.; Raghunath, P.; Lin, M. C. Effect of Roaming Transition States upon Product Branching in the Thermal Decomposition of CH_3NO_2. *J. Phys. Chem. A* **2013**, *117*, 7308-7313.

(35) Green, W. H.; Allen, J. W.; Buesser, B. A.; Ashcraft, R. W.; Beran, G. J.; Class, C. A.; Gao, C.; Goldsmith, C. F.; Harper, M. R.; Jalan, A.; Keceli, M.; Magoon, G. R.; Matheu, D. M.; Merchant, S. S.; Mo, J. D.; Petway, S.; Raman, S.; Sharma, S.; Song, J.; Suleymanov, Y. V.; Van Geem, K. M.; Vandeputte, A. G.; Wen, J.; West, R. H.; Wong, A.; Wong, H.-W.; Yelvington, P. E.; Yee, N.; Yu, J. *RMG - Reaction Mechanism Generator*, https://github.com/GreenGroup/RMG-Py, **2014.**

(36) Kohn, D. W.; Clauberg, H.; Chen, P. Flash Pyrolysis Nozzle for Generation of Radicals in a Supersonic Jet Expansion. *Rev. Sci. Instrum.* **1992**, *63*, 4003-4005.

(37) Rohrs, H. W.; Wickhamjones, C. T.; Ellison, G. B.; Berry, D.; Argrow, B. M. Fourier-Transform Infrared-Absorption Spectroscopy of Jet-Cooled Radicals. *Rev. Sci. Instrum.* **1995**, *66*, 2430-2441.

(38) Zhang, X.; Friderichsen, A. V.; Nandi, S.; Ellison, G. B.; David, D. E.; McKinnon, J. T.; Lindeman, T. G.; Dayton, D. C.; Nimlos, M. R. Intense, Hyperthermal Source of Organic Radicals for Matrix-Isolation Spectroscopy. *Rev. Sci. Instrum.* **2003**, *74*, 3077-3086.

(39) Urness, K. N.; Guan, Q.; Golan, A.; Daily, J. W.; Nimlos, M. R.; Stanton, J. F.; Ahmed, M.; Ellison, G. B. Pyrolysis of Furan in a Microreactor. *J. Chem. Phys.* **2013**, *139*, 124305.

(40) Steacie, E. W. R.; Shaw, G. T. The Homogeneous Unimolecular Decomposition of Gaseous Alkyl Nitrites. II. The Decomposition of Ethyl Nitrite. *J. Chem. Phys.* **1934**, *2*, 345.

(41) Levy, J. B. The Thermal Decomposition of Ethyl Nitrite. *J. Am. Chem. Soc.* **1956**, *78*, 1780-1783.

(42) Batt, L.; Milne, R. T. Gas-Phase Pyrolysis of Alkyl Nitrites. IV. Ethyl Nitrite. *Int. J. Chem. Kinet.* **1977**, *9*, 549-565.

(43) CHEMKIN-MFC, MFC 5.0. Reaction Design: San Diego, **2010**.

(44) Zhang, Y. J.; Cai, J. H.; Zhao, L.; Yang, J. Z.; Jin, H. F.; Cheng, Z. J.; Li, Y. Y.; Zhang, L. D.; Qi, F. An Experimental and Kinetic Modeling Study of Three Butene Isomers Pyrolysis at Low Pressure. *Combust. Flame* **2012**, *159*, 905-917.

(45) Fernández-Ramos, A.; Martínez-Núñez, E.; Ríos, M.A.; Rodríguez-Otero, J.; Vázquez, S.A.; Estévez, C.M. Direct Dynamics Study of the Dissociation and Elimination Channels in the Thermal Decomposition of Methyl Nitrite. *J. Am. Chem. Soc.* **1998**, *120*, 7594-7601.

(46) Heazlewood, B. R.; Jordan, M. J. T.; Kable, S. H.; Selby, T. M.; Osborn, D. L.; Shepler, B. C.; Braams, B. J.; Bowman, J. M. Roaming is the Dominant Mechanism for Molecular Products in Acetaldehyde Photodissociation. *Proc. Natl. Acad. U. S. A.* **2008**, *105*, 12719-12724.

(47) Harding, L. B.; Georgievskii, Y.; Klippenstein, S. J. Roaming Radical Kinetics in the Decomposition of Acetaldehyde. *J. Phys. Chem. A* **2010**, *114*, 765-777.

(48) Guan, Q.; Urness, K. N.; Ormond, T. K.; David, D. E.; Ellison, G. B.; Daily, J. W. The Properties of a Micro-Reactor for the Study of the Unimolecular Decomposition of Large Molecules. *Submitted to Int. J. Phys. Chem.* **2014**.

(49) Batt, L. Gas-Phase Decomposition of Alkoxy Radicals. *Int. J. Chem. Kinet.* **1979**, *11*, 977-993.

(50) Manion, J. A.; Huie, R. E.; Levin, R. D.; Burgess Jr., D. R.; Orkin, V. L.; Tsang, W.; McGivern, W. S.; Hudgens, J. W.; Knyazev, V. D.; Atkinson, D. B.; Chai, E.; Tereza, A. M.; Lin, C.-Y.; Allison, T. C.; Mallard, W. G.; Westley, F.; Herron, J. T.; Hampson, R. F.; Frizzell, D. H. NIST Chemical Kinetics Database, NIST Standard Reference Database 17, Version 7.0 (Web Version), Release 1.4.3, Data version 2008.12. http://kinetics.nist.gov

(51) Curran, H. J. Rate Constant Estimation for C_1 to C_4 Alkyl and Alkoxyl Radical Decomposition. *Int. J. Chem. Kinet.* **2006**, *38*, 250-275.

(52) Vasiliou, A. K.; Piech, K. M.; Reed, B.; Zhang, X.; Nimlos, M. R.; Ahmed, M.; Golan, A.; Kostko, O.; Osborn, D. L.; David, D. E.; Urness, K. N.; Daily, J. W.; Stanton, J. F.; Ellison, G. B. Thermal Decomposition of CH_3CHO Studied by Matrix Infrared Spectroscopy and Photoionization Mass Spectroscopy. *J. Chem. Phys.* **2012**, *137*, 164308.

(53) Pickett, H. M.; Poynter, R. L.; Cohen, E. A.; Delitsky, M. L.; Pearson, J. C.; Muller, H. S. P. Submillimeter, Millimeter, and Microwave Spectral Line Catalog. *J. Quant. Spectrosc. Radiat. Transfer* **1998**, *60*, 883-890, http://spec.jpl.nasa.gov

(54) Western, C. M. *PGOPHER, a Program for Simulating Rotational Structure*, University of Bristol: http://pgopher.chm.bris.ac.uk

(55) Susnow, R. G.; Dean, A. M.; Green, W. H.; Peczak, P.; Broadbelt, L. J. Rate-Based Construction of Kinetic Models for Complex Systems. *J. Phys. Chem. A* **1997**, *101*, 3731-3740.

(56) EFRC foundation kinetic model v.0.9. Hai Wang, private communication.

(57) Dean, A. M.; Bozzelli, J. W. Combustion Chemistry of Nitrogen. In *Gas-Phase Combustion Chemistry*, Gardiner, W. C., Ed. Springer: **2000**; pp 125-341.

(58) Zhang, K. W.; Zhang, L. D.; Xie, M. F.; Ye, L. L.; Zhang, F.; Glarborg, P.; Qi, F. An Experimental and Kinetic Modeling Study of Premixed Nitroethane Flames at Low Pressure. *Proc. Combust. Inst.* **2013**, *34*, 617-624.

(59) Lucassen, A.; Zhang, K. W.; Warkentin, J.; Moshammer, K.; Glarborg, P.; Marshall, P.; Kohse-Hoinghaus, K. Fuel-Nitrogen Conversion in the Combustion of Small Amines Using Dimethylamine and Ethylamine as Biomass-Related Model Fuels. *Combust. Flame* **2012**, *159*, 2254-2279.

(60) Lopez, J. G.; Rasmussen, C. L.; Alzueta, M. U.; Gao, Y.; Marshall, P.; Glarborg, P. Experimental and Kinetic Modeling Study of C_2H_4 Oxidation at High Pressure. *Proc. Combust. Inst.* **2009**, *32*, 367-375.

(61) Chang, A. Y.; Bozzelli, J. W.; Dean, A. M. Kinetic Analysis of Complex Chemical Activation and Unimolecular Dissociation Reactions Using QRRK Theory and the Modified Strong Collision Approximation. *Z. Chem. Phys.* **2000**, *214*, 1533-1568.

(62) Allen, J. W.; Goldsmith, C. F.; Green, W. H. Automatic Estimation of Pressure-Dependent Rate Coefficients. *Phys. Chem. Chem. Phys.* **2012**, *14*, 1131-1155.

(63) Benson, S. W. *Thermochemical Kinetics: Methods for the Estimation of Thermochemical Data and Rate Parameters*. **1976**.

(64) Welty, J.; Wicks, C.; Wilson, R.; Rorrer, G. *Fundamentals of Momentum, Heat, and Mass Transfer*. Wiley: **2000**.